Astronomy and Computing 44 (2023) 100714

Contents lists available at ScienceDirect

Astronomy and Computing

journal homepage: www.elsevier.com/locate/ascom

Full length article

Proving "new physics" by measuring cosmic ray fluxes

A. Chilingarian *, G. Hovsepyan

Yerevan Physics Institute, Alikhanyan Brothers 2, Yerevan, 0036, Armenia

ARTICLE INFO

Article history:
Received 1 February 2023
Accepted 17 May 2023
Available online 25 May 2023

ABSTRACT

Radiation on Earth's surface has been measured for more than a century using different particle detectors. These detectors have evolved from electroscopes to sophisticated, thousands-ton LHC detectors. Recently, with the availability of cheap particle detectors and simple data acquisition systems, publications have attempted to link changes in detector count rate to various astrophysical phenomena. However, measurement errors, meteorological conditions, and disturbances of electrical and geomagnetic fields can significantly impact cosmic ray fluxes. Some authors overlook these factors and publish "unique" correlations between their detector count rates and events such as solar and lunar eclipses, lightning strokes, Venus's transit over the Sun, and others.

When searching for the causes of cosmic ray enhancements, carefully distinguishing the atmospheric, instrumental, and astrophysical effects is essential. This paper aims to demonstrate how analyzing different species of cosmic ray flux can provide valuable insights into the underlying physical processes. We will explain how to verify that measurements are not due to abrupt changes in atmospheric conditions or equipment malfunctions but rather evidence of a novel physical phenomenon. Our goal is to provide a clear path from measurement to physical inference.

Experiments provide the basis for scientific knowledge.

1. Proof in physics

Physics is an inductive discipline that accepts some assumptions, gathers empirical results, compares them with other experiments and theories, and comes to new inferences explaining physical phenomena.

Standard dictionaries' definitions of "proof":

- The pieces of evidence that compel the mind to accept an assertion as true.
- Argument establishing a fact or the truth of a statement.
- The process of establishing the validity of a statement, especially by derivation from other statements following principles of reasoning.

In physics, scientific proof relies on experiments that convince the community of the accuracy of measurements and inferences. Established procedures exist for presenting, discussing, confirming, and validating statements, inferences, and theories based on measurements. In this article, we will use the measurement of cosmic ray fluxes on the earth's surface as an example to demonstrate these procedures. Our ultimate goal is to prove that changes in atmospheric pressure or temperature, equipment failure, or detector accuracy do not cause the peaks observed in the time series. Instead, we aim to show that they are a new physical phenomenon that can be further studied to develop a model and theory for their origin. To clarify the procedure, we need to define the problem. We need to identify any unusual event in the atmosphere or space that may have affected the count rate of cosmic rays, which we measure using particle detectors on the Earth's surface. We must analyze the recorded fluxes to determine if the changes in the count rate (whether it has decreased or increased) result from a new physical effect or simply random fluctuations or standard processes, such as a sudden change in atmospheric pressure.

To ensure accurate results, it is crucial to thoroughly examine all factors affecting the count rate, make appropriate adjustments, and determine how the detector reacts to various particles. When presenting findings related to new physics based on your measurements, it is essential to consistently revisit all potential sources of experimental errors to support your conclusions and explanations.

2. Particle detectors

Many different particle detectors register various types of cosmic rays. However, we aim to refrain from reviewing sensors or discussing how particles interact with the measuring media. Instead, we aim to explain the proper methodology for using acquired data to make physical inferences—in other words, to prove

* Corresponding author.
E-mail address: chili@aragats.am (A. Chilingarian).

https://doi.org/10.1016/j.ascom.2023.100714
2213-1337/

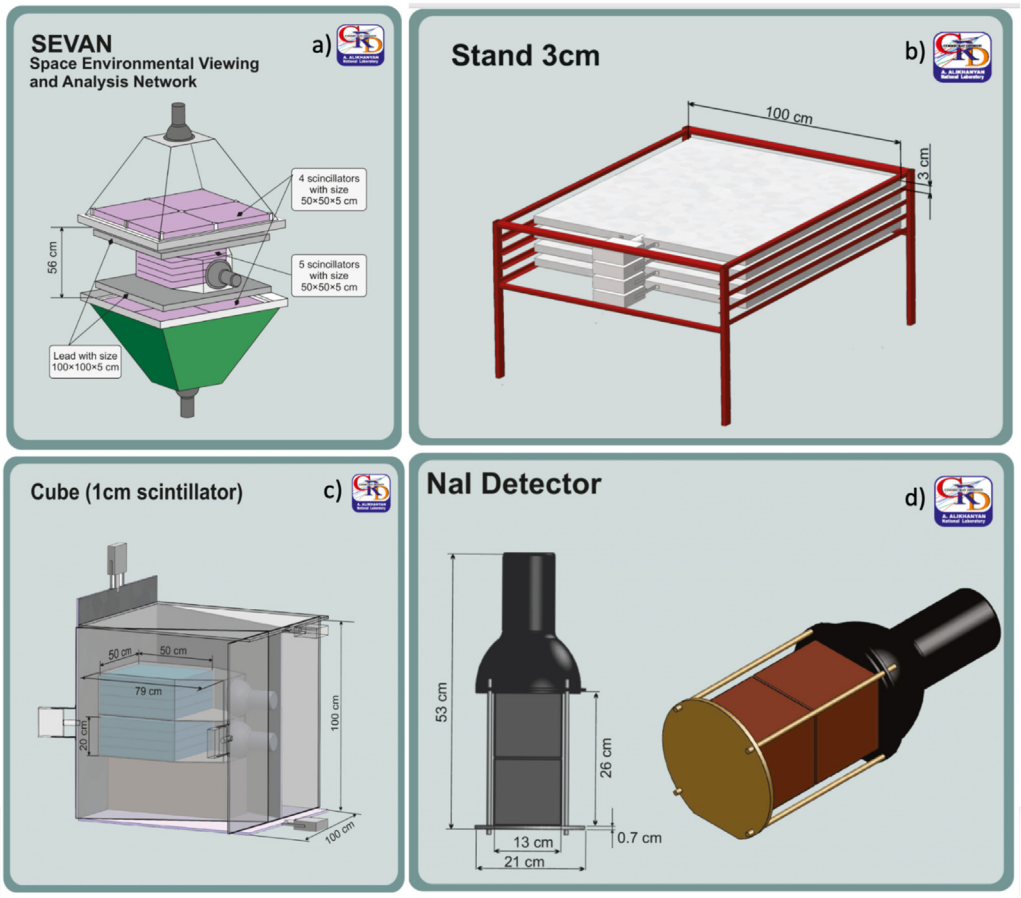

Fig. 1. Particle detectors operated on Aragats.

that we have measured a genuine signal from a new physical process. To illustrate this, we will use examples based on measurements taken at the Aragats cosmic ray observatory (Chilingarian et al., 2003). We will provide only minimal information on the detector's operation and refer to data that can be easily downloaded in graphical and numerical formats from the cosmic ray division (CRD) database of the Yerevan Physics Institute (YerPhI) (Anon, 2011).

In Fig. 1, we show particle detectors operated on Aragats. The SEVAN detector (Fig. 1a, details in Chilingarian et al. 2018) is built from standard plastic scintillators of 50 × 50 × 5 cm^3 size. Between two identical assemblies of 100 × 100 × 5 cm3 scintillators (four standard slabs arranged horizontally) are located two 100 × 100 × 5 cm^3 lead absorbers and a thick 50 × 50 × 25 cm^3 scintillator stack (5 standard slabs arranged vertically). Lights capture cones and photomultipliers (PMTs) are overviewed scintillator layers. In the upper 5 cm thick scintillator, charged particles are effectively registered; however, more substance must be used to register neutral particles. When a neutral particle traverses the upper scintillator, usually, no signal is produced. Incoming neutral particles undergo nuclear reactions in the thick 25 cm plastic scintillator, producing charged particles. The absence of the signal in the upper scintillators, coinciding with the signal in the middle scintillator, indicates neutral particle traversal (gamma-ray or neutron).

DAQ electronics register and store all logical combinations of the detector signals for further offline analysis and online alerts issuing. If we denote by "1" the signal from a scintillator and by "0" the absence of a signal, then the following combinations of the 3-layered detector output are possible: "111" and "101"—traversal of high energy muon; "010"—traversal of a neutral particle; "100"—traversal of low energy charged particle that stopped in the upper scintillator or the first lead absorber (energy less than ≈100 MeV). "110"—traversal of a charged particle of higher energy, which stopped in the second lead absorber. "001"—registration of inclined charged particles or very high energy gamma rays. DAQ electronics allow the remote control of the PMT high voltage and other parameters. The total weight of the SEVAN detector, including steel frame and detector housings, is ≈1,5 tons. 10 SEVAN detectors operate in Armenia, mountain tops of Eastern Europe, and Germany.

The "STAND3" detector comprises four layers of 3-cm-thick, 1-m^2 sensitive area scintillators stacked vertically see Fig. 1b. The light from the scintillator through optical spectrum-shifter fibers is reradiated to the long-wavelength region and passed to the photomultiplier (PMT FEU-115M). The maximum luminescence is emitted at the 420-nm wavelength, with a luminescence time of about 2.3 ns. The STAND3 detector is tuned by changing the high voltage applied to the PMT and setting the shaper-discriminator's thresholds. The discrimination level is chosen to guarantee signal detection at the maximum possible suppression of photomultiplier noise. Coincidences of the signals from 4 layers allow selecting charged particles with energy thresholds from 10 MeV ("1000" coincidence, the signal only in the upper layer) to >40 MeV ("1111" coincidence, signals in all layers)

The CUBE detector (Fig. 1c) consists of two 20-cm thick scintillators of 0.25-m^2 area each, enfolded by 1 cm thick, 1-m^2 area scintillators. This design ensures that no charged particle may hit the inside 20 cm without hitting the surrounding "veto" scintillators. The 20-cm thick plastic scintillators are overviewed by the photomultiplier PM-49 with a large cathode operating in a low-noise regime. Surrounding detectors (six units) are 1-cm

thick molded plastic scintillators. The efficiency of registration of neutral particles by 1-cm thick scintillators is 1%–2% and weakly depending on their energy. The energy losses of electrons in a 20-cm-thick plastic scintillator are ∼40 MeV. Considering the construction material of the detector (2-mm iron tilt and 1-cm plastic scintillator) and the roof of the building (0.8-mm iron tilt), the energy threshold of the upper 20-cm-thick scintillator is estimated to be about 10 MeV and for the bottom one ∼40 MeV. The efficiency of gamma ray registration in a 20 cm thick scintillator equals ∼20%, and the neutron detection efficiency is ∼27%.

The NaI(Tl) crystal used for spectrometry (shown in Fig. 1d) is enclosed in a sealed aluminum casing that is 3 mm thick. The crystal is coated on all sides with 0.5 cm of magnesium oxide (MgO) and has a transparent window that faces the photocathode of a PMT of FEU-49 type. The PMT's spectral sensitivity range of 300–850 nm covers the spectrum of light emitted by NaI(Tl). Crystal has a sensitive area of approximately 0.035 m^2 and a 60%–80% gamma-ray detection efficiency. The FEU-49 signals are coded using a logarithmic analog-digital converter (LADC), calibrated by a 137Cs isotope emitting 662 keV gamma rays, and the muon peak appeared in the histogram of energy releases. The PMT high voltage was adjusted to ensure linearity of LADC in the energy region of 0.3–50 MeV, covering both extremes in the histogram of LADC output signals. Additionally, the sensitive volume of the detector is protected from electrons with energy lower than ∼3 MeV by the substance above it (0.7 mm of roof tilt, 3 mm of aluminum, and 5 mm of MgO). Therefore, the network of NaI spectrometers can only detect gamma rays below 3 MeV, which is very useful in research of Radon progeny gamma radiation.

3. Detector response function, purity and efficiency of the detector, and detector response to charged and neutral CR species

Any sensor's detection rate is affected by various factors such as its size, location, and registration efficiency. Atmospheric pressure, temperature, NSEF, geomagnetic field, and solar wind also impact the count rate. Additionally, the count rate could be influenced by power supply oscillations, diurnal and seasonal variations, and the random nature of physical processes utilized for particle detection, such as PMT noise.

To derive parameters having physical meaning, we have to deconvolute the measured count rate to be not dependent on the specific characteristic of the detector, estimate different particle fluxes and energy spectra as they were before entering the detector, and estimate measurement errors.

Analyzing how the particle detector registers elementary particles is essential to ensure accurate results. Without understanding the detector's response, particle flux measurements will be arbitrary, and any physical inference will be unreliable. This is known as the direct problem of CR. The ideal way to solve this is through particle beam calibrations on artificial accelerators, but this option is only sometimes readily available. Alternatively, we can use CR flux generators like EXPACS (Sato, 2016) to give us flux data for all CR species across all latitudes, longitudes, and altitudes, combined with the GEANT4 code (GEANT4 collaboration, 2003) for particle tracking. However, it is important to remember that the inevitable simplification of a model will affect the recovered particle fluxes and could impact the reliability of any physical inferences drawn from it. For more information on how to make physical inferences based on simulations, please refer to the methodology outlined in Chilingarian (2004).

Table 1 displays the purity of the STAND3 detector coincidences achieved with EXPACS and GEANT4 packages. EXPACS provides the flux of all CR species at Aragats station, while GEANT4 tracks all particles that enter the detector setup. EXPACS provides the flux of all cosmic ray species at Aragats station, while GEANT4 follows all particles that enter the detector setup. As demonstrated in Table 1, each scintillator coincidence selects specific frequencies of background composition that differ from the actual composition obtained by EXPACS (first column). To get the particle frequencies, we need to solve the inverse cosmic ray problem by using the measured composition to recover the genuine one. Nonetheless, we can expand the selection of different elementary particles by choosing other trigger options for the STAND3 detector. The "1000" coincidence selects approximately 51% neutral particles, "1111" coincidence selects muons (about 77%), and "1110" selects low energy muons, electrons, and positrons (about 80%).

Table 1
Purity of the STAND3 coincidences measuring the ambient population of secondary cosmic ray flux (background) flux on Aragats (3200 m) in percent.

Particle	Purity (%)				
	EXPACS	1000	1100	1110	1111
n	18.6	17.22	5.83	2.20	0.48
p	1.5	4.37	7.42	7.28	6.23
μ+	6.8	5.01	12.21	23.03	41.28
μ-	6	4.52	11.08	20.04	35.92
e-	6.2	21.31	24.77	19.95	6.85
e+	3.6	13.44	18.62	15.67	6.67
γ	57	33.57	20.07	11.83	2.57

Table 2
Efficiency (%) of electron registration by STAND3 detector.

STAND3	1000	1100	1110	1111	Sum
10 MeV	81.23	0.01	0.00	0.00	81.25
12 MeV	89.34	0.10	0.00	0.00	89.43
14 MeV	91.45	0.29	0.00	0.00	91.73
16 MeV	87.28	5.22	0.00	0.00	92.50
18 MeV	69.97	22.72	0.00	0.00	92.69
20 MeV	50.43	42.23	0.03	0.00	92.70
30 MeV	13.08	57.41	20.73	0.03	91.26
40 MeV	6.22	25.89	47.18	10.29	89.58
50 MeV	4.10	14.10	33.13	37.47	88.79
60 MeV	3.08	9.41	22.86	53.19	88.54

To recover the genuine particle flux entering the detector, we need to estimate the registration efficiency, i.e., the percent of the registered particles relative to the entered detector. We utilized the EXPACS and GEANT4 packages to calculate the efficiency of electrons and gamma rays in the 1–50 MeV energy range. Table 2 shows the energy dependence of the electron registration efficiency for the STAND3 detector. The table reveals that the detector's efficiency is heavily influenced by the energy of the electron. For instance, the "1000" coincidence effectively selects electrons with energies between 10–20 MeV, while the "1100" coincidence is effective with energies between 20–30 MeV. The "1110" coincidence works best with energies between 30–40 MeV, and the "1111" coincidence is optimal for energies above 50 MeV.

Table 3 displays the efficiencies of gamma ray detection using the STAND3 detector. From the table, it is evident that the efficiency of gamma ray detection is relatively low. We can employ STAND3's 1110 and 1111 coincidences to separate the mixed electron-gamma flux. Comparing the efficiencies presented in Tables 1 and 2, we can deduce that if there are noticeable peaks in the time series of these coincidences, the electron flux reaching the ground is substantial.

4. The influence of the atmospheric parameters on the particle detector count rates

Measurements of the different species of secondary cosmic rays have been ongoing for 80 years at Aragats station. NaI and

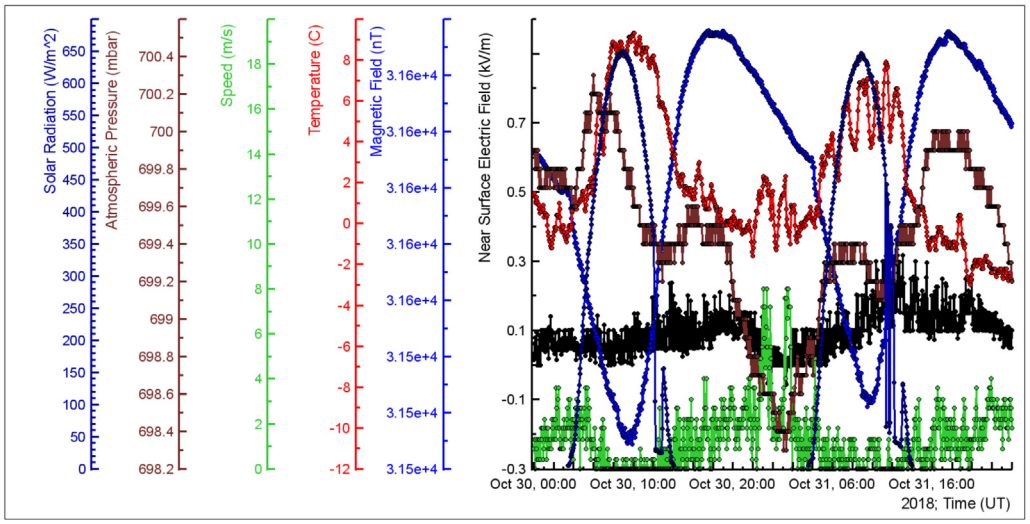

Fig. 2. Time series of environmental parameters influencing particle detector count rates. Black—NSEF; blue—geomagnetic field; red—outside temperature; green—wind speed; magenta—atmospheric pressure.

Table 3
Efficiency (%) of gamma rays registration by STAND3 detector.

STAND3	1000	1100	1110	1111	Sum
10 MeV	5.81	0.03	0.00	0.00	5.84
20 MeV	4.55	2.35	0.02	0.00	6.92
30 MeV	2.06	4.22	0.89	0.01	7.18
40 MeV	0.83	3.56	2.52	0.37	7.28
50 MeV	0.44	2.37	3.16	1.50	7.47
60 MeV	0.29	1.43	3.10	2.83	7.65

scintillation spectrometers are used to recover energy spectra. NaI and plastic scintillators measure electrons, muons, and gamma rays. Neutron monitors and SEVAN detectors are used to measure neutrons, and the muon detector and neutron monitor are also used to measure extensive air showers' cores.

The Davis Vantage Pro2 weather station has a rain collector, temperature sensor, humidity sensor, anemometer, solar radiation sensor, ultra-violet (UV) radiation sensor, and other tools to measure weather conditions.

LEMI-018 vector magnetometer is used to measure the three components of the geomagnetic field. Near-surface electrostatic field changes are monitored by a network of six field mills (Boltek EFM-100), with three located in Aragats station, one in Nor Amberd station 12.8 km away, one in Burakan 15 km away, and one in Yerevan 39 km away. All data is fed into the Advanced data extraction infrastructure (ADEI) operated at databases of CRD/YerPhI, which provides vast possibilities for multivariate visualization and correlation analysis.

Fig. 2 displays atmospheric parameters that affect the count rate of particle detectors. The most significant parameters include outside temperature (red), atmospheric pressure (magenta), and NSEF (black). Count rate bias caused by atmospheric effects can exceed 10%, more than usually the subtle effects expected from astrophysical sources. Therefore, special corrections must be made to distinguish possible "new physics" from simple count rate biases of atmospheric nature.

In Fig. 3, we display how NSEF and temperature impact the count rates of NaI detectors. When thunderstorms occur, NSEF (black curve) lifts charged aerosols with attached Radon gas isotopes. The gamma radiation emitted by the lifted radon isotopes (mainly 214Pb and 214Bi) boosts the count rate of the NaI detector for approximately 2–3 h (left side of Fig. 3). Around ten hours later, a mighty wind electrifies the metallic plates of sensor EFM 100, resulting in multiple pulses that appear as a thick black band in the NSEF time series. These fluctuations do not affect the count rate as they are solely an instrumental effect. Subsequently, temperature changes between day and night, reaching ≈10°C (red curve), significantly impact the count rate fluctuations. The count rate of the NaI crystal is heavily influenced by temperature, and the detector is situated beneath a metallic roof. On sunny days, the temperature inside the building rises quickly, causing the count rate (blue curve) to increase correspondingly. The shift between the outside temperature and count rate takes roughly 3.5 h as it requires time to heat the metallic roof and transfer the heat to the inside of the building.

Fig. 4 illustrates a "delayed" correlation analysis of time series. As depicted in Fig. 3, when the internal temperature of the building housing the NaI detector increases, the detector's count rate increases by about 10%. Fig. 4 shows the time series of solar irradiance, the count rate of the NaI detector, and the outside temperature. The peak values of solar irradiance and outside temperature coincide, but there is a noticeable delay between the outside temperature and count rate, as indicated by green lines. To estimate the delay between temperature and count rate, we employed "delayed" correlation techniques. We shifted the time series by one-minute intervals and calculated the correlation coefficient for each delay, resulting in a delayed correlation curve, as shown in the inset of Fig. 4. The maximum correlation occurs at ≈3.5 h.

In turn, the count rate of scintillation detectors is anti-correlated with the temperature and is most influenced by atmospheric pressure. Thus, several overall and detector-dependent reasons exist for the count rate variations. All of them should be carefully examined before discussing a physical inference based on the CR measurements.

5. Statistical moments of measured count rates, relative errors, and significance of detected peaks. Gaussian nature of random errors

To study the characteristics of the detector, it is essential to select a time when the weather conditions are relatively stable and do not significantly impact the detector's count rate. The statistical moments of the count rates can be estimated through sample means and variances. After calculating the means and variances of the time series, we must determine whether any peaks that appeared in the time series are within acceptable statistical limits

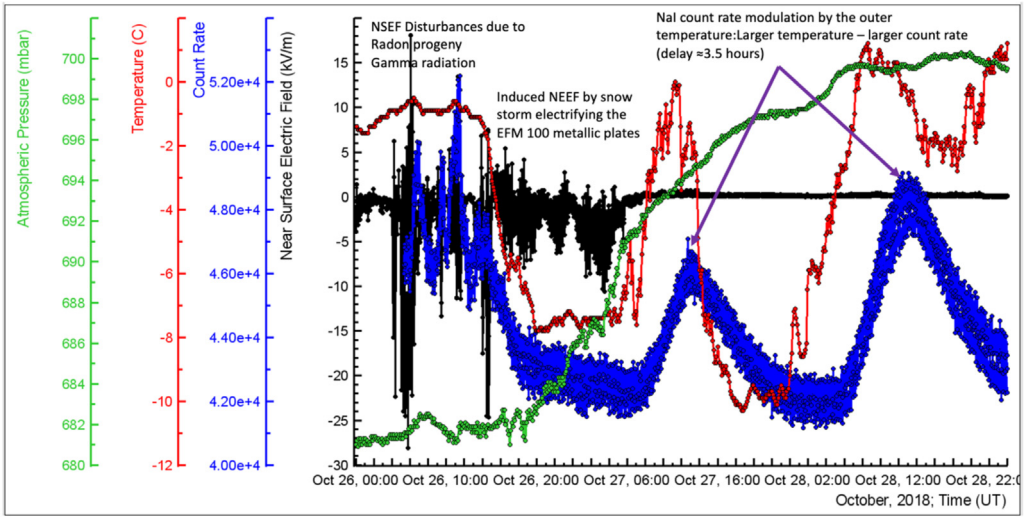

Fig. 3. 1-min time series of NaI detector's count rates (blue), influenced by NSEF disturbances (black) and outside temperature (red). The influence of temperature on the count rate is overwhelming, and the impact of the significant atmospheric pressure variations (green) is not noticed.

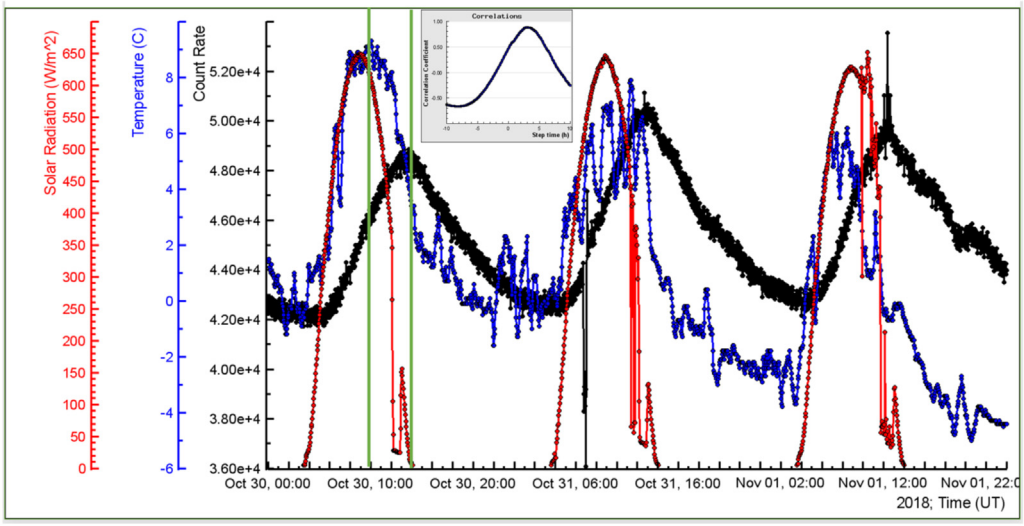

Fig. 4. 1 min count rate of NaI detector (black curve) influenced by outside temperature variations (blue curve). By the red curve, solar irradiation is shown. In the inset, we offer the delayed correlation curve.

or indicate a new phenomenon. We will demonstrate identifying genuine peaks, such as thunderstorm ground enhancements (TGEs) observed on Aragats (Chilingarian et al., 2022).

The summer of 2022 in Aragats was characterized by hot and dry weather. Among very few "summer TGEs", the highest recorded enhancement was only 8%. And the peak significance measured in standard deviations above fair-weather value was at most 10. However, on September 22, during a routine storm, the detectors unexpectedly detected 7 TGEs, 3 of which showed a significant flux enhancement, as depicted in Fig. 5, which displays the count rates of the STAND3 detector. We calculated the means and variances during fair weather conditions when all meteorological parameters were stable to quantify the flux enhancements (see Fig. 6).

The presented in Fig. 6 distributions, their means, variances, and relative errors provide a measure of sensitivity to the "new physics"; the relative errors outline the minimum signal value, which can be considered a possible artifact. The relative errors of STAND3 triggers are slightly different; however, a limit of 3% can be accepted as a conservative estimate for all 4. Count rate fluctuations within 3% cannot be taken as a significant deviation from the mean value to be examined for possible nontrivial signals.

Table 4
Simulated with EXPACS and GEANT4 and measured 1-min count rates of STAND3 coincidences.

STAND3/min	"1000"	"1100"	"1110"	"1111"
Simulation	7278	3235	2197	15328
Measurement	8617	3464	2463	12600

Table 4 compares the simulated and measured 1-min count rates of the STAND3 detector. The flux discrepancies are within 20%, which is satisfactory for the approximate background fluxes obtained from the WEB calculator Sato (2016) and for integrating the particle flux for a whole day, neglecting the so-called day-wave, the variation of the flux during a day due to changing meteorological conditions.

In Fig. 7, we show time series of count rates for all STAND3 detector triggers. The number of standard deviations (critical value, $N\sigma$) for each peak is calculated using data from Fig. 6. The most prominent peak, 82σ, corresponds to the lowest energy

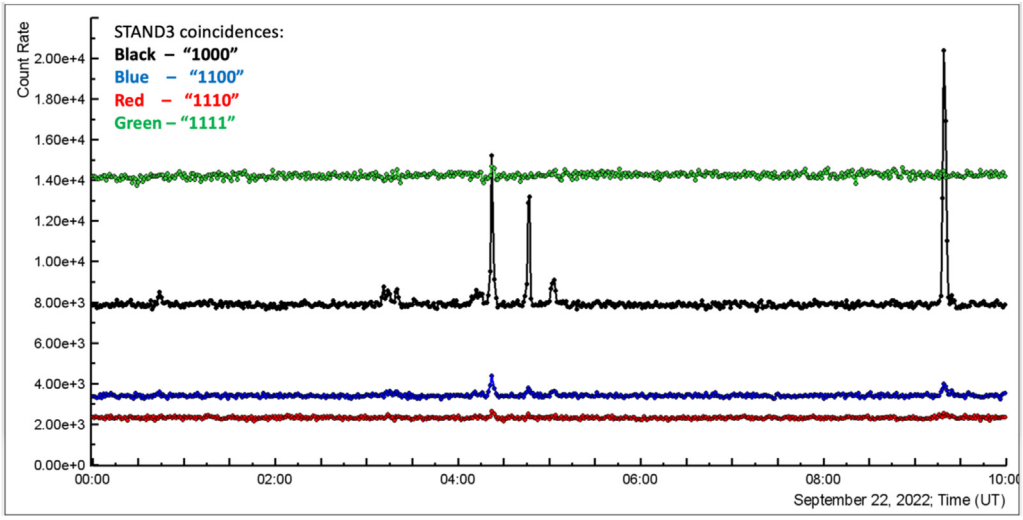

Fig. 5. 1-min time series of the count rates of STAND3 detector's coincidences.

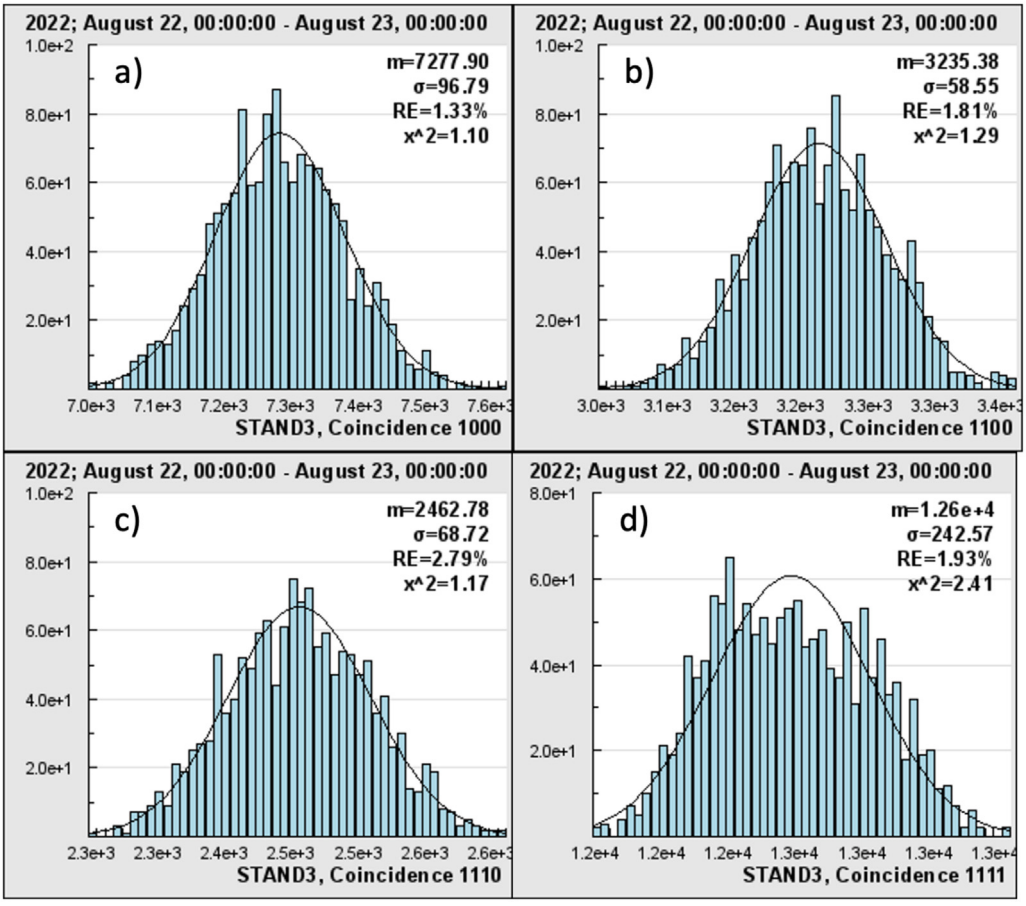

Fig. 6. Means, variances, and relative errors of STAND3 detector coincidences. The whole day August 22, 2022, 1440 min (no corrections to the atmospheric pressure and outside temperature are done).

threshold (STAND3's "1000" trigger). According to Neumann–Pearson's approach to statistical decisions (Lehmann, 1993), a critical value is fixed to accept or reject the so-called H0 hypothesis that all measurements belong to the Gaussian population (the process in control). Each critical value (usually set to 3 in medical research and 5 in elementary particle searches (Biglietti et al., 2022; Manzoni, 2019), see, Fig. 8) is connected to the so-called *p*-value, the integral of the Gaussian function from the critical value to infinity. To prove the existence of a signal, we have to reject H0 with the maximal possible confidence. However, significant deviations from H0, i.e., a very low probability of H0 being true, do not imply that the opposite hypothesis is automatically valid. As was mentioned by Astone and D'Agostini (Astone and D'Agostini, 1999), behind the logic of standard hypothesis testing is hidden a revised version of the classical proof by contradiction. "In standard dialectics", one assumes a hypothesis to be true,

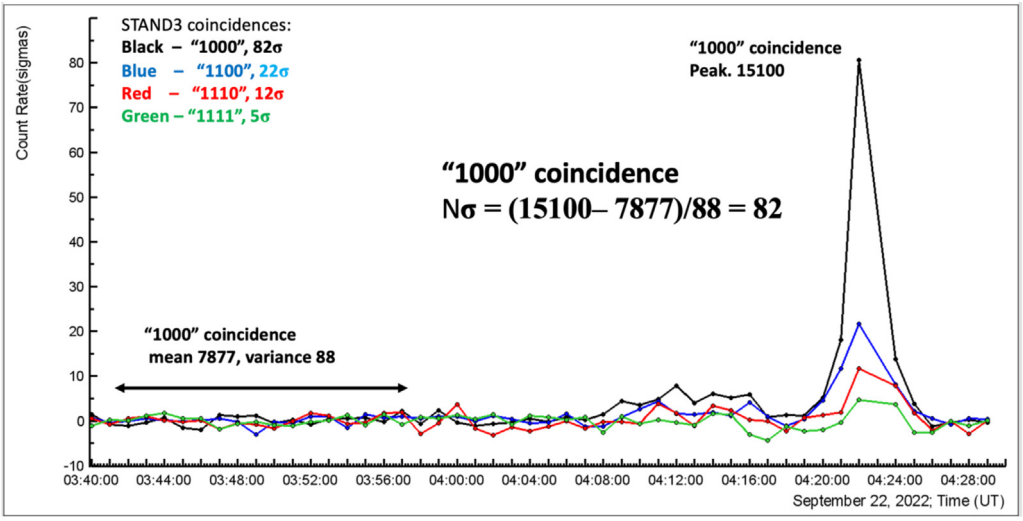

Fig. 7. 1-min time series of the count rates of STAND3 detector coincidences in numbers of standard deviations, critical value, $N\sigma$.

then looks for a logical consequence manifestly false, to reject this hypothesis. The "slight" difference introduced in the statistical tests is that a "very improbable consequence" replaced the false consequence.

To analyze the TGE that started at 04:22, we calculated the critical value based on the measured peak height, time series mean, and variance rather than fixing it. In Fig. 7, we present the critical value, which is much greater than 5, and the corresponding p-value indicating an extremely low chance probability of rejecting H0 erroneously.

In Fig. 9a, we display the probability associated with the critical value of $N = 5$ (used in high-energy physics), which is only one chance out of 3500 000. In Fig. 9b, the Gaussian integral from $N = 82$ (the peak significance in STAND3 detector) to infinity yields an incredibly tiny value of $3.8 * 10^{-1461.}$

You can find a comprehensive guide to data analysis for large astrophysical experiments in Abbott et al. (2020).

6. Observer's influence on the distribution function of measurements

Physicists conducting experiments often use selection criteria to choose a subset of data that contains exceptional measurements that differ significantly from the overall population. This approach is commonly used when searching for celestial objects emitting ultra-high energy cosmic rays, solar protons emitted during flares, or maximums in the invariant mass distribution in experiments on colliders. They then calculate the number of standard deviations from the mean value obtained under the H0 hypothesis, i.e.,$-N\sigma$. For the $N(0, 1)$ distribution, the chance probability of erroneously rejecting H0 (p-value) for the right-tailed test the p-value is calculated in the following way:

$$G^{>N} = \int_N^{\infty} e^{-\frac{x^2}{2}} dx \tag{1}$$

After conducting M different selections (cuts), physicists obtain a number of standard deviations $(Ni, i = 1, M)$ for each cut, corresponding to the minimal p-values. Then they select the largest $N_{\max}$ among these Ni values and substitute it in Eq. (1) instead of N to obtain a much smaller chance probability. Applying this method yields tiny probabilities of being wrong in searches of celestial sources of cosmic rays (Nie et al., 2022; Abraham et al., 2007), pentaquark (Seife, 2004), etc. However, this approach needs to consider that the distribution of $N_{\max}$ follows the binomial law.

$$f(k, m, p) = b(m, k)p^k(1 - p)^{m-k}, \tag{2}$$

where $b(m, k)$ is the binomial coefficient, k is the number of successful trials, p is the probability of a successful trial, and M is the total number of trials. For the case of selecting the maximum value ($N_{\max}$) from M trials, $k = 1$ and $p(k) = G{>}N_{\max}$. Thus, if performing multiple trials, the chance probability (erroneously rejecting H0) can be calculated using the equation (see details in Chilingarian et al., 2006; Chapman et al., 2002):

$$G^{>Nmax} = M * G^{>Nmax}(1 - G^{>Nmax})^{M-1}. \tag{3}$$

Eq. (3) and Eq. (1) yield significantly different chance probabilities. To illustrate an incorrect p-value calculation, we refer to a paper that attempted to enhance the detection of high-energy protons by the L3 detector during the July 14, 2000, solar flare. The original publication stated a number of standard deviation of $N = 4.2$ (Achard et al., 2006), while the revised calculation after 4100 cuts was $N = 5.7$ (Wang, 2009).

The muon drift-chamber system, located in a 1000 m^3 magnetic field of 0.5 T, was used to capture and measure the momentum of cosmic ray muons. These muons originated in interactions of protons accelerated during energetic solar events with the atmosphere. The L3+C detector system, based at CERN, combined high-precision muon drift chambers with an air shower array on the surface to detect these particles. The detector was near Geneva (6.02°E, 46.25°N), about 30 m underground. It covered a full geometrical acceptance of ∼200 m^2 sr, with a zenith angle range of 0° to 60°, and provided an average energy threshold of around 20 GeV for vertically incident muons.

The selected events were separated into specific intervals to analyze potential signals and sorted based on the direction of the arriving muon. After performing $42 * 100$ cuts and selecting $N_{\max} = 5.7$, the p-value calculated by Eq. (1) corresponds to a chance probability of approximately 6^*10^{-9}. However, by using the correct Eq. (3), which considers the M cuts needed to achieve N^{max}, the p-value is $2.5 * 10^{-4}$, equivalent to about $N = 4$ of Eq. (1). This is less than the initially reported value of $N = 4.2$.

7. Conclusions

To validate a significant enhancement of the cosmic ray flux (prominent peak in the time series of the detector's count rate),

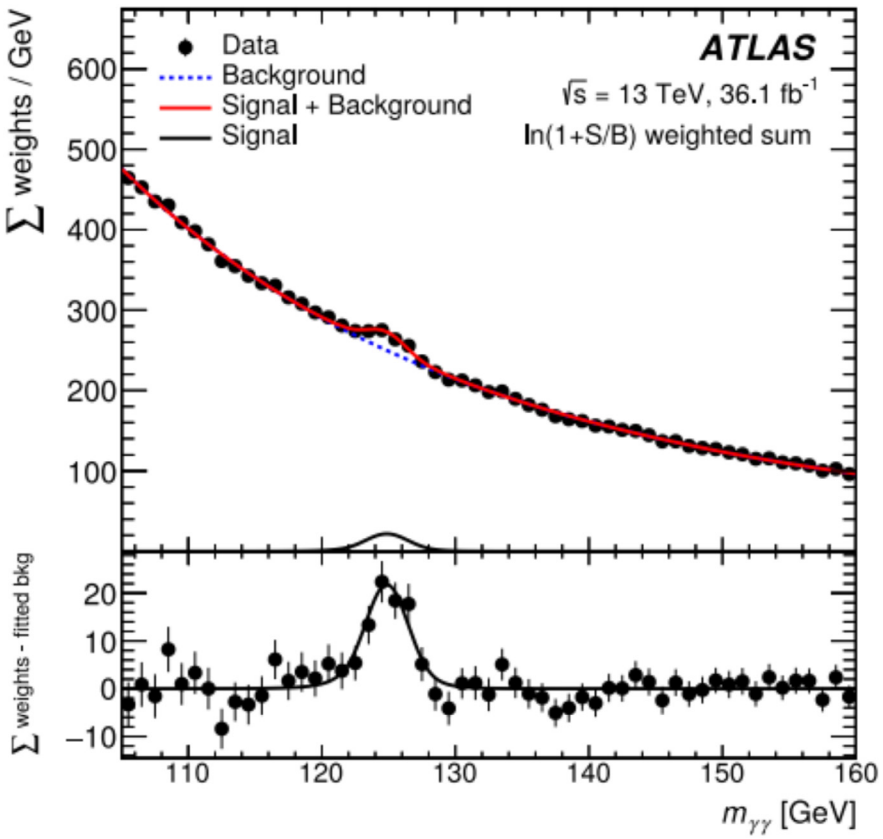

Fig. 8. The distribution of the invariant mass of the two photons in the ATLAS experiment at LHC. Measurement of H→$\gamma\gamma$ using the complete 2015+2016 data set. An excess is observed for a mass of ∼125 GeV. In the bottom panel—the background subtracted distributions.
Source: Adopted from Biglietti et al. 2022, *J. Phys.: Conf. Ser.* **1586** 012028.

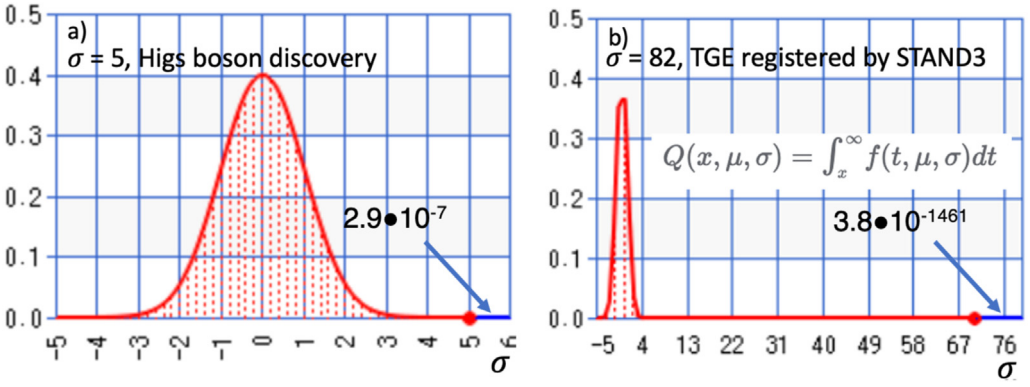

Fig. 9. Standard Gaussian distribution demonstrating the chance probability (blue lines) of Higgs boson evidence (a) and detection of TGE by STAND3 upper scintillator (b). Chance probability was calculated by the ke! san Online Calculator (https://keisan.casio.com/).

one must carefully consider all possible influences of atmospheric parameters, electronics or power outages, and random fluctuation on the particle detector count rate. This can be achieved by estimating the detector response function, comparing count rates of different detectors, monitoring atmospheric conditions, and calculating the chance probability of erroneous decisions. It is crucial to note that superimposed cuts on initial data could artificially lower the *p*-value and lead to incorrect results.

To establish the new physical phenomenon, it is essential to reveal its origin by measuring the energy spectra of electrons and gamma rays, performing simulations of particle propagation in the atmosphere, and comparing simulation and experimental data. Each step follows well-established procedures to ensure the correctness and soundness of the physical inference. At Aragats cosmic ray observatory, various particle detectors monitor CR fluxes and energy spectra simultaneously, allowing cross-calibration. Spectrometers measure electron and gamma ray energy spectra separately. Using these spectra and GEANT4 simulations, we calculate the expected count rates of electrons and gamma rays and compare them with the experimentally measured ones (Chilingarian et al., 2022, 2023).

In addition, Refs. Manzoni (2019), Abbott et al. (2020), Nie et al. (2022) contain exhaustive demonstrations of physical inference techniques, including proofs of the existence of the Higgs boson, gravitational waves, and the signal from the CRAB nebula detected by the LHAASO experiment.

Declaration of competing interest

The authors declare no conflict of interest.

Data availability

Data will be made available on request

Acknowledgments

Authors thank A. Kavalov and S. Chilingaryan for valuable discussions. The authors acknowledge the support of the Science Committee of the Republic of Armenia (research project № 21AG-1C012).

References

GEANT4 collaboration, 2003. GEANT4–a simulation toolkit. Nucl. Instrum. Methods A 506, 250.
Abbott, B.P., et al., 2020. A guide to LIGO–Virgo detector noise and extraction of transient gravitational-wave signals. Class. Quantum Grav. 37, 055002.
Abraham, et al., 2007. Correlation of the highest-energy cosmic rays with nearby active galactic nuclei positions. Astropart. Phys. 29 (2008), 188–204.
Achard, P., et al., 2006. The solar flare of the 14th of July 2000 (L3+C detector results). Astron. Astrophys. 456, 351.
Anon, 2011. CRD data analysis portal. Available online: http://adei.crd.yerphi.am/adei/ (Accessed 29 May 2023).
Astone, P., D'Agostini, G., 1999. Inferring the intensity of Poison processes at the limit of the detector sensitivity, CERN-EP/99-126.
Biglietti, et al., 2022. J. Phys.: Conf. Ser. 1586, 012028.
Chapman, S.C., Rowlands, G., Watkins, N.W., 2002. Extremum statistics – a framework for data analysis. Nonlinear Process. Geophys. 9, 409–418.
Chilingarian, A., 2004. Nonparametric methods of data analysis in cosmic ray astrophysics, an applied theory of Monte Carlo statistical inference. Available online: http://crd.yerphi.am/Monogram (Accessed 29 May 2023).
Chilingarian, A., Avagyan, K., Babayan, V., et al., 2003. Aragats space-environmental center: Status and SEP forecasting possibilities. J. Phys. G 29, 939.
Chilingarian, A., Hovsepyan, G., Aslanyan, D., Karapetyan, T., Khanikyanc, Y., Kozliner, L., Sargsyan, B., Soghomonyan, S., Chilingaryan, S., Pokhsraryan, D., Zazyan, M., 2022. Thunderstorm ground enhancements: Multivariate analysis of 12 years of observations. Phys. Rev. D 106, 082004.
Chilingarian, A., Hovsepyan, G., Karapetyan, T., Aslanyan, D., Chilingaryan, S., Sargsyan, B., 2023. Phys. Rev. D 107.
Chilingarian, A., Karapetyan, G., et al., 2006. Statistical methods for signal estimation of point sources of cosmic rays. Astropart. Phys. 25, 269–27615.
Lehmann, E.L., 1993. The Fisher, Neyman-Pearson theories of testing hypotheses: One theory or two? J. Amer. Statist. Assoc. 88, 1242.
Manzoni, S., 2019. Physics with Photons using the ATLAS Run 2 Data. Springer Theses, (ISSN: 2190-5053) ISBN: 978-3-030-24369-2, doi:10.1007/978-3-030-24370-8.
Nie, L., Liu, Y., Jiang, Z., Geng, X., 2022. Ultra-high-energy Gamma-ray radiation from the crab pulsar wind nebula. Astrophys. J. 924, 42.
Sato, T., 2016. Analytical model for estimating the zenith angle dependence of terrestrial cosmic ray fluxes. PLOS ONE 11, e0160390.
Seife, C., 2004. Rara avis, or statistical mirage? Pentaquark remains at large. Science 306, 1281.
Wang, R., 2009. Did the 2000 July 14 solar flare accelerate protons to P40 GeV? Astropart. Phys. 31, 149–155.